JOURNAL OF MATERIALS SCIENCE 39 (2004) 1343– 1355

Evolution of the main intermetallic phases in Al-Si-Cu-Mg casting alloys during solution treatment

L. LASA, J. M. RODRIGUEZ-IBABE
CEIT and Tecnun, P° M. de Lardizabal 15, 20018 San Sebastian, Basque-Country, Spain
E-mail: jmribabe@ceit.es

The effect of the copper content and the processing route in the solution treatment of four Al-Si-Cu-Mg alloys was studied. The solidus temperature of each alloy was obtained through differential scanning calorimetry (DSC) and compared with Thermo-Calc calculations. This temperature was between 509–510°C in all cases. In consequence, three temperatures were chosen for the solution treatment: 480, 490 and 500°C. An alternative two-step solution treatment finishing at 535°C was also adopted for the alloy with the lowest copper content. Solution times up to 24 h were considered. The dissolution of the intermetallic phases was measured using both, metallographic analysis and from the evolution of the DSC peaks. The results from the two methods were in good agreement. Thermo-Calc calculations helped explaining the changes in volume fraction of the main intermetallic phases observed during the solution treatments.

1. Introduction

Al-Si foundry alloys are extensively used in the automotive and the aerospace industry due to their excellent castability, good mechanical properties, and wear resistance [1, 2]. The addition of alloying elements such as magnesium and copper make these alloys heat treatable, further improving their mechanical properties and allowing their use in new, more demanding applications.

The most common thermal treatments used with these alloys involve either age hardening the as-cast alloy (T5-type) or solution treatment followed by age hardening (T6-type). For most applications, the T6 treatment is usually adopted because it produces maximum tensile strength and hardness. During the solution treatment, the alloy is subjected to high temperatures for relatively long periods of time with two main objectives: first, to obtain maximum solubility and homogeneity of the alloying elements and impurities in the matrix, and second, to modify the acicular morphology of the eutectic silicon to a less detrimental, rounded one [3].

The solution temperature must be high enough and the treatment time long enough to allow maximum dissolution and homogenization of the alloying elements. However, raising the temperature too much can lead to incipient melting of the alloy which affects the ductility of the alloy [4, 5]. The treatment time should be an optimum to achieve an effective dissolution and also to avoid the coarsening of the constituents [6].

One of the main problems inherent to Al-Si casting alloys is their high heat content that prolongs the solidification time, especially in the case of hypereutectic alloys. Different processing routes are currently employed with these alloys. Processes with a slow cooling rate produce segregation and lead to growth of intermetallic phases, whereas a fast cooling rate minimizes nucleation and growth of the precipitates. Depending on the alloy composition and cooling rate, a high degree of matrix saturation can be obtained, making possible the use of short solution treatments. In fact, when peak mechanical properties are not required, processes with high enough cooling rates may allow suppressing the solution treatment step altogether, obtaining very significant hardening during artificial aging and greatly reducing the production cost [7, 8].

The presence of certain impurities, or the addition of alloying elements outside the optimum levels, can produce insoluble phases during solidification. It can be difficult or even impossible to dissolve these phases during the solution treatment thereby, reducing its effectiveness. Since the choice of processing route also controls the formation of intermetallic phases during solidification and cooling, the thermal treatments and alloy compositions must be tailored to each specific processing route, in order to obtain the desired final mechanical properties [9]. In this study, alloys produced in three different ways were considered: conventional permanent mould casting, lost foam and thixoforming.

Conventional casting in permanent moulds is very widely used. The solidification rate is rather high and sound parts with low porosity levels and good mechanical properties are relatively easily produced.

Using the lost foam process very intricate castings with excellent surface finish can be obtained [10].

Another important advantage of this process is that there is no need for expensive metallic moulds. The main drawbacks are the low solidification rate and the residual porosity formed during the degradation of the polymeric pattern [11].

The thixoforming process drastically reduces the casting temperature, and consequently the heat content, because the alloys are processed containing around 0.4–0.6 solid fraction. The solidification time is shorter and the resulting microstructure is fine and homogeneous. The very special microstructure obtained after thixoforming gives rise to the excellent mechanical properties and wear behavior of thixoformed Al-Si alloys [12, 13]. High cost and the impossibility of recycling scraps in the same production plant are two of the main problems associated with this processing route. These problems are currently being addressed by the introduction of the so called New RheoCasting process (NRC) [14–16].

The very different processing routes employed in the production of the four alloys considered in this work produced remarkable changes in the identity, volume fraction and morphology of the intermetallic phases in the as-received alloys.

The main purpose of this work is to determine the optimum parameters of the solution treatments for each alloy and to relate them to the different microstructures of the as-cast alloys. Another objective is to study the evolution of the different intermetallic phases during solution treatment done at different temperatures.

2. Experimental procedure

The chemical composition of the alloys and their processing routes are shown in Table I. Alloys H3 and H4 were cast in the form of rectangular specimens weighing 0.6 Kg. each by Hydro Aluminum (Norway). Alloy E was produced by Hydro and later cast using lost-foam technology by CR-FIAT (Italy). Finally, the thixotropic alloy Thixo477 was produced by Pechiney (France) and thixoformed by The University of Sheffield (U.K.).

The thermal treatments were carried out in a salt bath using small rectangular specimens of $15 \times 10 \times 20$ mm approx., cut from the central part of thick sections. The temperature variation in the salt bath remained always within $\pm 2^{\circ}$C of the temperature set. After solution treatment, the samples were immediately quenched in water at room temperature and polished following standard metallographic practices. Finally, Keller's reagent was used to achieve maximum contrast of the constituents. A minimum of 24 pictures at 500× magnification of the polished and etched specimens were taken in the

TABLE I Chemical composition and processing route of the alloys

		Chemical composition (%)					
Alloy	Processing route	Si	Mg	Cu	Ni	Fe	Ti
H3	Perm. mould	12.85	1.30	1.37	0.00	0.11	0.11
H4	Perm. mould	12.29	1.30	4.40	0.00	0.12	0.11
E	Lost-foam	12.64	1.09	4.39	0.00	0.19	0.13
Thixo477	Thixoforming	15.30	0.58	4.38	<0.42	0.21	0.16

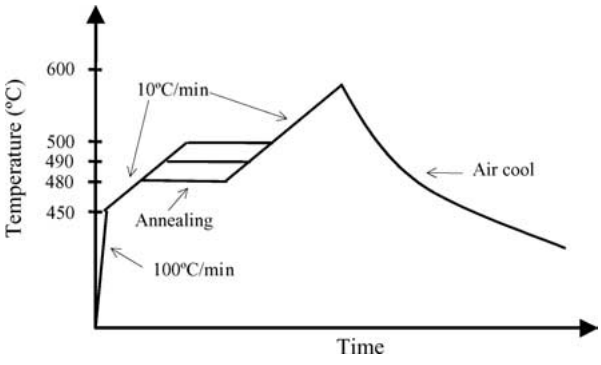

Figure 1 Heating cycle of the solution treatments done in the DSC chamber.

scanning electron microscope (SEM) using back scattered electrons (BSE); 1000× magnification was used for alloy Thixo477 due to its finer microstructure. Four intermetallic phases were quantified: Al_2Cu (θ), Mg_2Si (β), $Al_5Mg_8Cu_2Si_6$ (Q) and $Al_8FeMg_3Si_6$ (π). These phases were identified using EDS analysis in the SEM.

The optimum color-contrast permitted the use of computer based image analysis to quantify the intermetallic phases Al_2Cu (θ) (SEM) and Mg_2Si (β) (optical microscope). The other two phases were quantified using the point count method.

Small cylindrical discs, 4 mm in diameter and 0.45 mm in thickness with an approximate weight of 15 mg were cut for the differential scanning calorimetry (DSC) experiments. The reference material was annealed high purity aluminum and the baseline was subtracted from the data. Nitrogen was used as protective atmosphere. The heating cycles applied in the DSC chamber are shown in Fig. 1.

Initially a high heating rate of 100°C/min was used up to 450°C. Once this temperature was reached, the heating rate was limited to 10°C/min. The reproducibility of the DSC runs was checked by repeating some of the cycles.

Thermo-Calc software [17] was used to calculate the solidus temperature and the stability and evolution of the different phases with temperature. The program uses a database to calculate the minimum Gibbs energy for a specific system. The calculations done in this study correspond to the equilibrium conditions at each temperature. The database used, TTAL [18], is specifically designed for use with aluminum alloys. All the possible intermetallic phases were included in the calculations.

3. Results and discussion

3.1. Microstructure

The microstructures of the four as-received alloys are shown in Fig. 2. In the figures, the eutectic and primary silicon particles are dark gray. The different intermetallic phases are concentrated mainly in the interdendritic spaces and are light gray in color, with the exception of Mg_2Si (β) which is black. In Fig. 3a SEM picture of the main intermetallic phases together with their EDS spectra is shown.

Alloys H3 and H4 showed a very similar distribution and size of the eutectic and primary silicon particles.

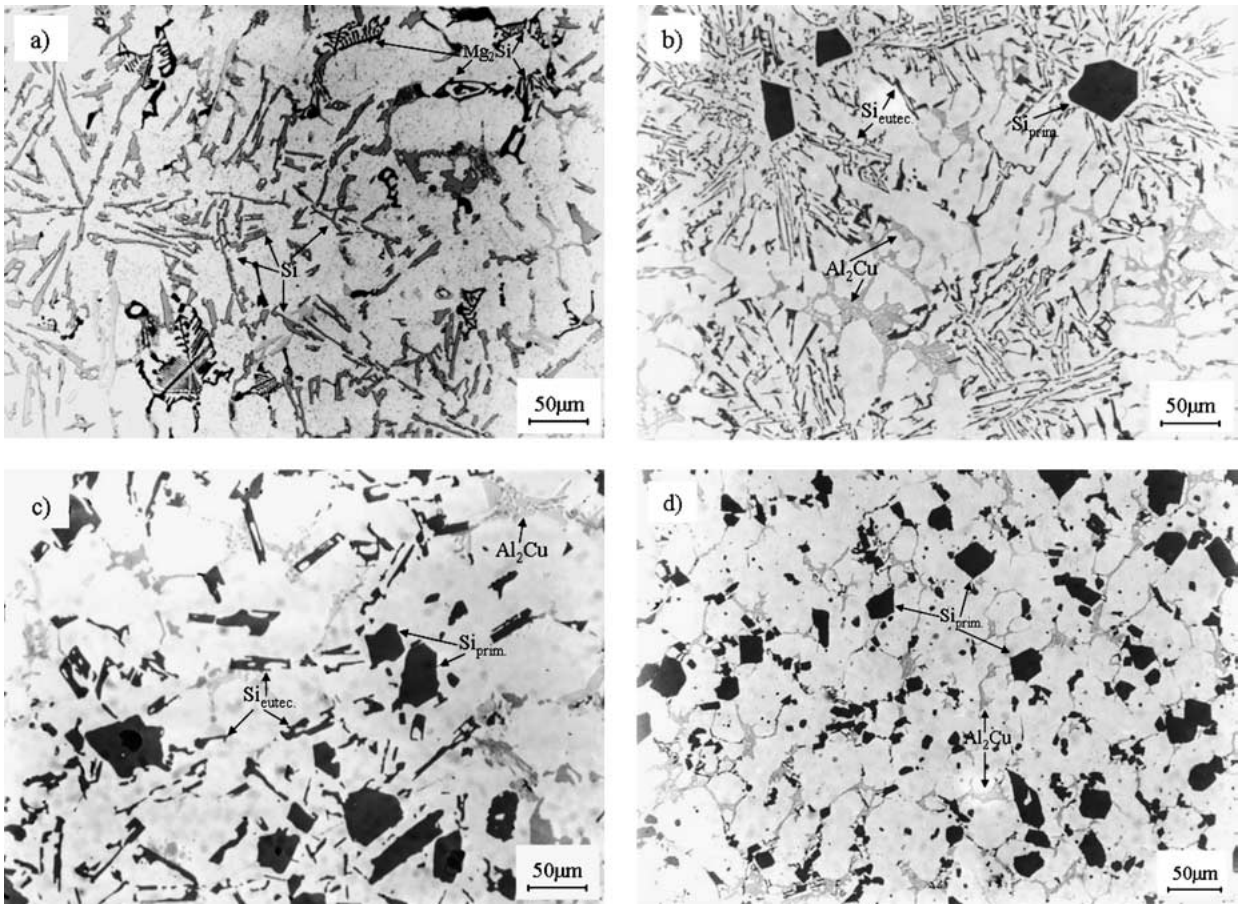

Figure 2 Microstructure of the four alloys: (a) alloy H3, (b) alloy H4, (c) alloy E, and (d) alloy Thixo477.

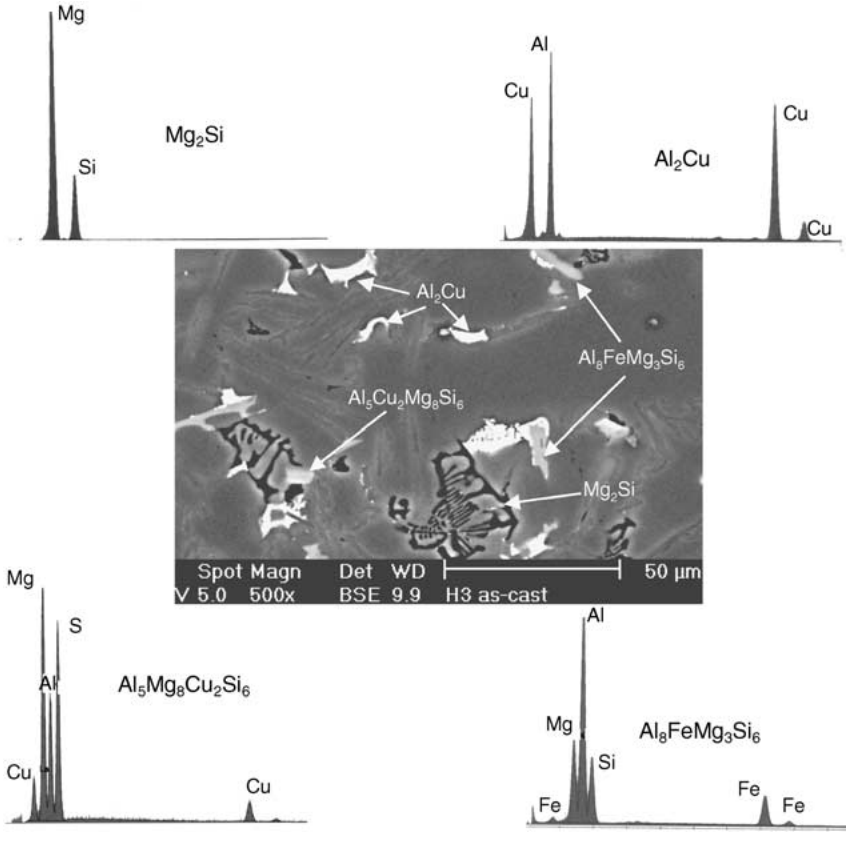

Figure 3 Detail of the intermetallic phases in alloy H3 with their corresponding EDS analysis.

TABLE II Metallographic measurements and theoretical values of the main intermetallic phases in the as-received condition

	Intermetallic phases (%)							
	Al_2Cu (θ)		Mg_2Si (β)		$Al_5Si_6Cu_2Mg_8$ (Q)		$Al_8FeMg_3Si_6$ (π)	
Alloy	Exp.	Theor.	Exp.	Theor.	Exp.	Theor.	Exp.	Theor.
H3	0.9 ± 0.1	1.48	1.7 ± 0.4	2.40	0.1 ± 0.3	0	0.9 ± 0.2	0.96
H4	3.6 ± 0.5	3.71	0	0	1.5 ± 0.2	3.60	0.7 ± 0.2	1.05
E	4.5 ± 0.6	4.03	0	0	1.1 ± 0.2	2.65	1.4 ± 0.4	1.66
Thixo477	4.7 ± 0.4	4.63	0	0	[a]	0.96	[a]	1.84

[a]The size of the particles was small and no quantitative measurements could be made.

However due to the significantly lower copper content of alloy H3, the identity and percentage of the intermetallic phases present in the two alloys were very different. Alloy H3 presented mainly Mg_2Si (β) in the Chinese script form (see Fig. 2a). In alloy H4 the main intermetallic phase was Al_2Cu (θ), concentrated at the grain boundaries and triple points of the aluminum dendrites (see Fig. 2b).

The microstructure of alloy E is shown in Fig. 2c. The composition of this alloy is very similar to that of alloy H4, and there was no big difference in the as-received microstructures of the two alloys. However, the microstructure of alloy E was somewhat coarser due to the slower solidification rate of the lost foam process. As in alloy H4, most of the intermetallic phases were distributed along the grain boundaries, but in alloy E, some smaller θ particles (<1 μm) were also found inside the aluminum phase.

The thixoformed alloy Thixo477 shows a completely different microstructure (see Fig. 2d) from the other 3 alloys. The aluminum phase was rounded, the silicon particles smaller and of polygonal shape, and the intermetallic phases extremely fine, distributed evenly around the aluminum globules.

The metallographic measurements of the volume fractions of the different intermetallic phases in the alloys in the as-received condition are shown in Table II. Also in this table, the possible maximum fractions of the intermetallic phases calculated using mass balance are shown. It should be noted that the compositions of alloys H4, E and Thixo477 are similar with only small differences in the percentage of alloying elements and impurities. Those differences together with the processing routes were responsible for the changes in the volume fractions of the intermetallic phases measured.

For the calculations it was considered that all the iron is attracted by the π phase and that the remaining magnesium goes to the Q phase in alloys H4, E and Thixo477 and to the β phase in alloy H3. In the case of the π phase the differences between calculated and measured values are small.

In alloys H4, E and Thixo477 the difference is explained by the morphology and distribution of the particles of the Q phase. Most of this phase is in the form of isolated polygonal particles and the rest forming a fine complex eutectic together with the θ phase (Fig. 4). During the metallographic measurements, often it was not possible to distinguish it form the θ phase. Thus part of the θ phase measured metallographically corresponds to the Q phase. In alloy H3 the calculated

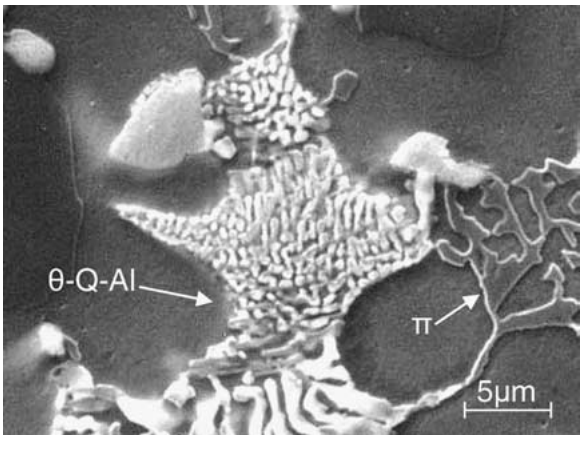

Figure 4 Morphology of the θ-Q-Al eutectic in alloy Thixo477.

percentages of the θ and Q phases are high because the presence of the Q phase is not considered in the calculations. If a percentage of the Q phase is allowed the calculated values come close to the measured ones.

An additional reason for the differences observed, is that despite the relatively slow cooling rate of the production of the parts, the matrix still keeps some degree of supersaturation that is not taken into account in the calculations.

The DSC scans of the as-received alloys are shown in Fig. 5. The DSC scans allowed the determination of the solidus temperature of the alloys (the temperature at which the first eutectic melts). This temperature defined the upper limit for the solution heat treatments. In the figure, the solidus temperature of the alloys obtained by Thermo-Calc is also shown.

The solidus of the four alloys as determined by DSC was between 509–510°C. All alloys, with the exception of alloy H3, presented a well defined peak at this temperature that considering the composition of the alloys it corresponds to reaction (1) [19].

$$Al + Si + Al_2Cu(\theta) + Al_5Mg_8Cu_2Si_6(Q) \rightarrow \text{Liquid} \quad (1)$$

The area under the peak in alloy H3 was small and it even did not appear when slower heating rates were employed (5°C/min or less), demonstrating that θ, Q or both phases dissolved at high temperatures, effectively delaying the solidus until 540°C.

In alloys H4, E and Thixo477, a small depression of the DSC curve was observed prior to the first

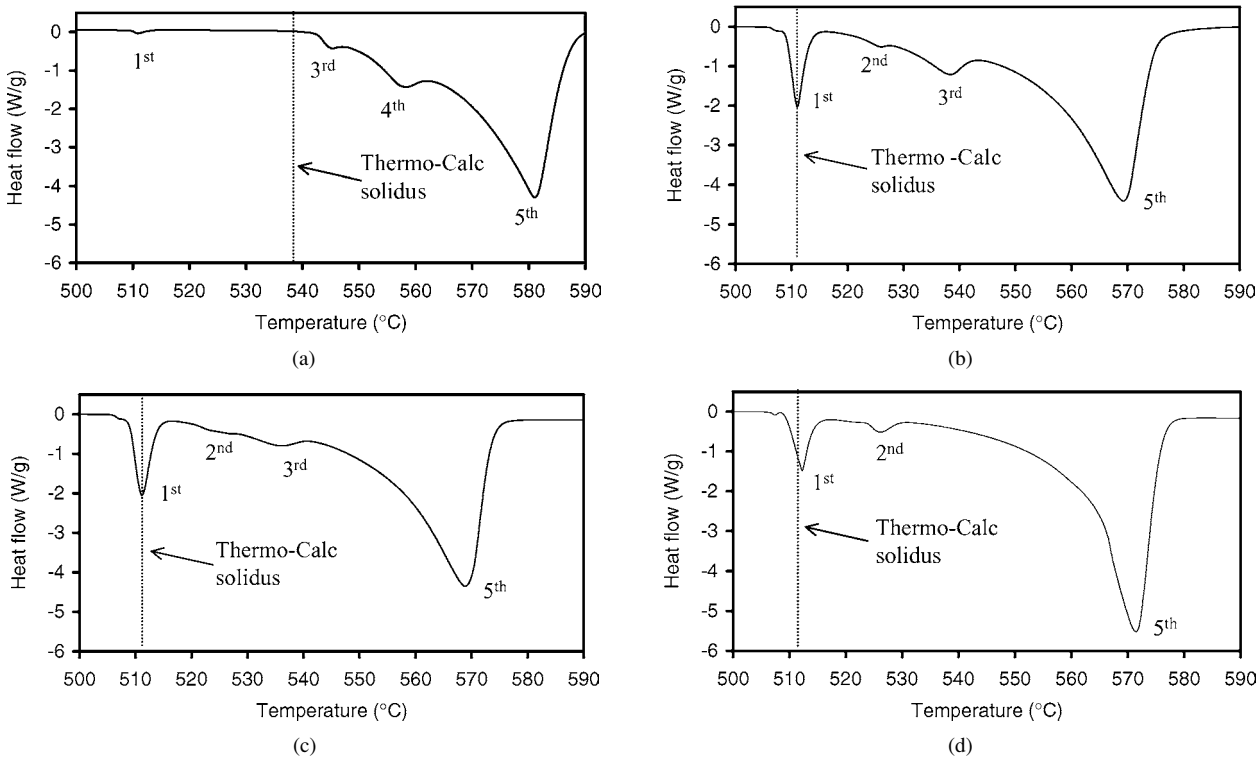

Figure 5 DSC scans of the alloys as-received: (a) alloy H3, (b) alloy H4, (c) alloy E, and (d) alloy Thixo477. The dotted lines represent the solidus calculated by Thermo-Calc.

endothermic peak. This peak is most likely produced by reaction (2):

$$Al + Al_2Cu(\theta) + CuMgAl_2 \rightarrow \text{Liquid} \qquad (2)$$

According to [20] this reaction takes place at 507°C. The $CuMgAl_2$ usually forms in low silicon content alloys but it could be present in small amounts in the alloys studied producing the small peak observed in the DSC runs.

The DSC scans were also used to identify the intermetallic phases present in each alloy together with their melting points.

In Table III, the possible reactions for each DSC peak as predicted by Mondolfo [20] for Al-Si-Cu-Mg alloys are listed. These reactions were selected considering the composition of the alloys and the temperature at which each of the DSC peaks took place.

In order to assign a single reaction to each DSC peak, the data from metallographic measurements, DSC scans and Thermo-Calc calculations were combined. In Fig. 6 the evolution of the main phases with temperature calculated by Thermo-Calc is given. The $TiAl_3$ phase is not included because the amounts predicted are very low in all the alloys.

The calculations were mainly used to analyze the stability of the intermetallic phases during the solution treatments but they also provided valuable information about the temperatures at which the different phases dissolved or reacted. These data have been used for the identification of the DSC peaks.

Regarding the first DSC peak, different authors agree in attributing it to reaction (a) in Table III [21, 22]. In alloys E, H4 and Thixo477, the alloys with higher copper content, the amount of θ and Q phases measured metallographically was considerable. In alloy H3 the amount of θ phase was very small and consequently the energy of the first peak was smaller than in the higher copper content alloys. However it must be remembered that the peak area does not only depend on the amount of phase transformed but also on the transformation enthalpy.

TABLE III Possible reactions for each DSC peak predicted by Mondolfo [19]

DSCpeak	Mondolfo		*T* (°C)
1st (509–510°C)	$Al + Si + Al_2Cu + Al_5Mg_8Cu_2Si_6 \rightarrow$ liquid	(a)	507
2nd (525–527°C)	$Al + Al_5Mg_8Cu_2Si_6 \rightarrow$ liquid $+ Si + Mg_2Si$	(b)	529
	$Al + Al_2Cu + Si \rightarrow$ liquid	(c)	525
3rd (530–542°C)	$Al + Al_5Mg_8Cu_2Si_6 \rightarrow$ liquid $+ Si + Mg_2Si$	(b)	529
	$Al + Mg_2Si + Si \rightarrow$ liquid	(d)	555
	$Al + Mg_2Si + Si + Al_8FeMg_3Si_6 \rightarrow$ liquid	(e)	554
4th (550–551°C)	$Al + Mg_2Si + Si \rightarrow$ liquid	(d)	555
	$Al + Mg_2Si + Si + Al_8FeMg_3Si_6 \rightarrow$ liquid	(e)	554
5th (552–562°C)	$Al + Si \rightarrow$ liquid	(f)	577
	$Al + Si + Al_8FeMg_3Si_6 \rightarrow$ liquid + Mg 2Si	(g)	567

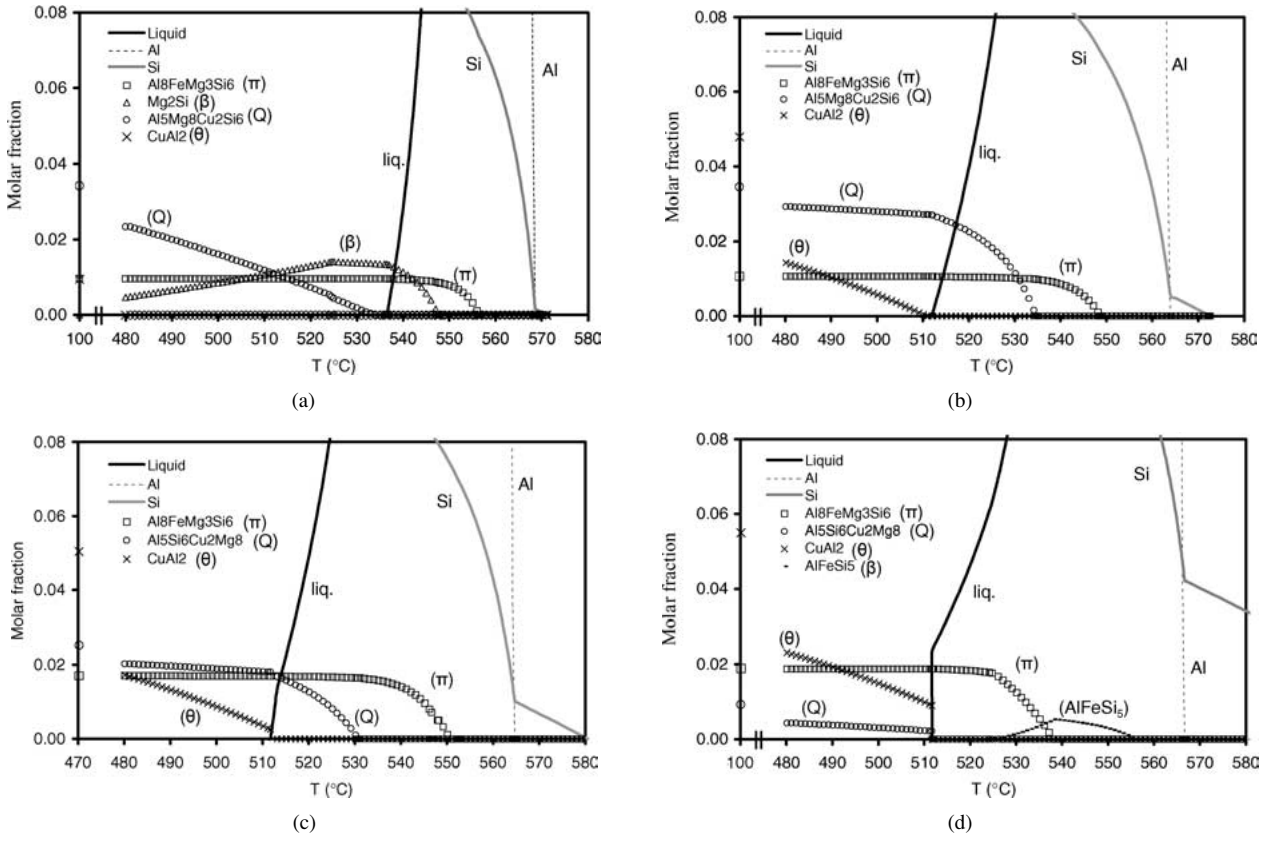

Figure 6 Evolution of the main intermetallic phases as calculated by Thermo-Calc: (a) alloy H3, (b) alloy H4, (c) alloy E, and (d) alloy Thixo477.

The Thermo-Calc calculations also confirmed the identity of this peak, as shown in Fig. 6. In alloys E, H4 and Thixo477, the θ and Q phases were stable until 510°C. At this temperature, they reacted with aluminum and silicon forming liquid (reaction (a)). In alloy H3, on the other hand, Thermo-Calc predicted that the θ phase is only stable at low temperatures (<300°C). In the DSC runs a peak was obtained because during the relatively fast heating the system is far from equilibrium. At slower heating rates the θ phase has time to dissolve in alloy H3, and hence reaction (1) would not occur.

The second peak in alloys E, H4 and Thixo477 could be produced by reactions (b) or (c) (Table III). Supposing that the peak corresponds to reaction (b), the energy of the DSC peak should be proportional to the amount of Q phase found in each alloy, that is, highest in alloy H4 and lowest in alloy Thixo477. However, the energy of the peak followed the opposite trend. Consequently, the second peak was attributed to reaction (c).

The energy of the third peak was higher in alloy H4 than in alloy E due to the higher amount of Q phase measured in the former when compared to the latter. In alloy Thixo477 this peak did not occur. This result is not surprising because the amount of Q phase was considerably smaller in this alloy, due its lower magnesium content and relatively high Fe content that favor the formation of π phase instead (see Fig. 6). Hence, the third peak in alloys H4 and E was produced by reaction (b). In alloy H3, the Thermo-Calc calculations suggest that the second DSC peak also corresponds to reaction (b).

The fourth peak was only observed in alloy H3. According to Thermo-Calc calculations, at the temperature where the peak took place (around 550°C) the β phase reacts with silicon and aluminum producing more liquid (reaction (d)). The high copper content of alloys E, H4 and Thixo477 eliminated the presence of the β phase as measured metallographically and also calculated by Thermo-Calc. Consequently the 4th peak did not take place in these three alloys.

Finally, regarding to the 5th peak, it is well known that this peak corresponds to the main eutectic reaction (f). From Thermo-Calc calculations, the $Al_8FeMg_3Si_6$ phase (π) also melts at the same temperature (reaction (g)). The 5th DSC peak is produced simultaneously by reactions (f) and (g) (Table III).

In many cases, reaction temperatures predicted by Thermo-Calc differ slightly from the values obtained experimentally. However, the differences are in most cases small and Thermo-Calc proves to be useful in these alloy systems.

3.2. Solution treatment

As was mentioned before, three temperatures were chosen for the solution treatments: 500, 490 and 480°C. In the case of alloy H3, a two step solution treatment, finishing at 535°C, was also adopted.

Since the peaks in the DSC runs were already identified, as described in the previous section, it was possible to relate the changes in the peak energies during the solution treatments to the dissolution or formation of specific intermetallic phases. The results from the DSC runs were compared to direct measurements of the intermetallic phases using metallographic means.

The temperature of the solution treatment dictates the solubility of the alloying elements in the aluminum matrix. From Thermo-Calc calculations, in alloys H4, E and Thixo477, the solubility of copper increases steeply with temperature up to approx. 4% at 500°C. The increase in magnesium solubility is more moderate; in these alloys, only 0.25% can be placed in solution at 500°C. In alloy H3 all the copper can be dissolved at 490°C. The solubility of Mg at 500°C is only 0.29%. However, at 535°C up to 0.40% magnesium and 1.30% silicon can be dissolved. It is extremely important to maximize the solubility of Mg in these alloys because the hardening effect of this element, even in small concentrations, is very strong [23, 24].

However, those are equilibrium solubilities. The dissolution rate of the intermetallic phases varies with the processing route and composition of the alloy and it may not be possible to attain the equilibrium solubility in a given alloy. In any case, the time at the nominal solution temperature should be long enough to allow maximum dissolution of the alloying elements.

The optimum solution treatment time was considered to be the time needed to obtain equilibrium dissolution of the intermetallic phases. Longer times do not produce further solubilization and only coarsen the microstructure.

3.2.1. Alloy H3

The results for the evolution of the main intermetallic phases during solution treatment in permanent mould cast alloy H3 are shown in Fig. 7. The curves for the θ phase are not included because this intermetallic phase dissolved immediately during the solution treatment.

The evolution of the Q phase measured metallographically and by DSC was very similar. In the as-received condition, the amount of this intermetallic phase was very small. During solution treatment, a progressive formation of this intermetallic was observed, reaching a stationary situation after about 5 h. However, at equilibrium, the amount of Q phase decreased when the solution temperature was raised, being minimum at the two step solution treatment finishing at 535°C.

The β phase dissolved very fast during solution treatment. Even after just 2 min at the lowest solution temperature (480°C), it reached a state of equilibrium dissolution. The extremely fast dissolution made the DSC highly inaccurate. During the heating cycle in the DSC chamber, the β phase quickly dissolved and the energy of the peak did not correspond to the amount of β phase measured metallographically.

The evolution of the β and Q intermetallic phases during the solution treatment was opposite. During the processing, the alloy solidified fast, outside equilibrium conditions. According to Thermo-Calc calculations (Fig. 6) the β phase forms at high temperatures, and even if its stability decreases as the temperature goes down, the relatively fast cooling rate does not allow significant dissolution levels of this intermetallic phase. The opposite situation was found with the Q phase. This intermetallic phase starts to form at around 533°C and gains stability as the temperature goes down. In any case, Thermo-Calc predicts the phases present at each temperature, under equilibrium solidification conditions, only found under extremely slow cooling rates. At high cooling rates, there is no time for the precipitation of the Q phase explaining why only small amounts

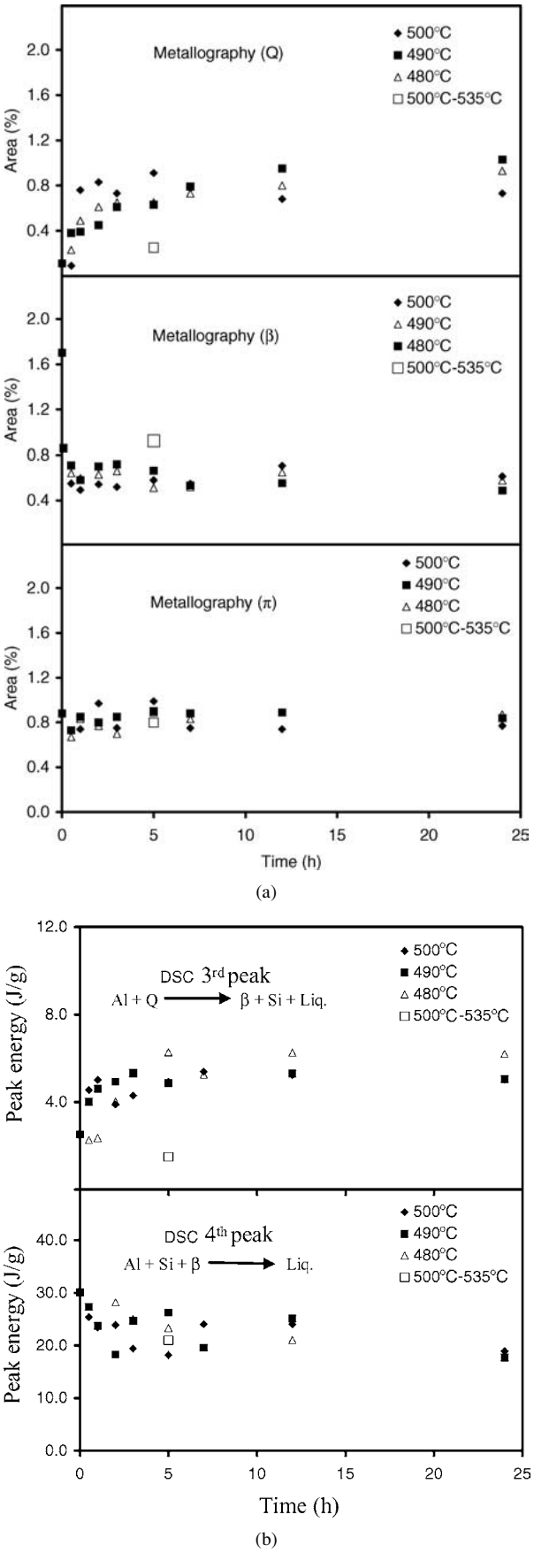

Figure 7 Evolution of the main intermetallic phases in alloy H3: (a) metallography and (b) DSC.

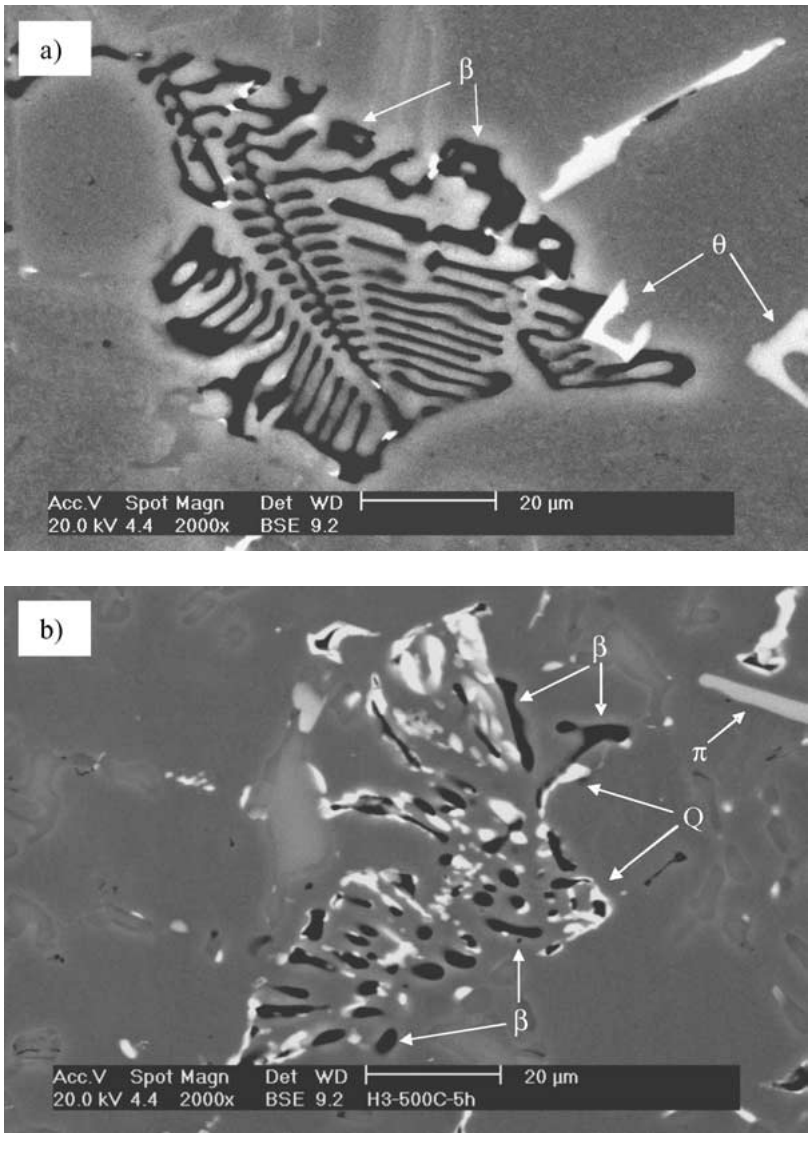

Figure 8 Dissolution of the β phase and precipitation of the Q phase in alloy H3 during solution treatment: (a) alloy as cast and (b) after 5 h at 500°C.

were found in the alloy as-received. During solution treatment, the alloy progressively approximated equilibrium at each solution temperature; the β phase started to dissolve while simultaneously, increasing amounts of the Q phase were nucleated in the particles of the β phase. This transformation is shown in the two micrographs of Fig. 8. Fig. 8a is a detail of the as-cast microstructure showing a particle of the β phase with the typical Chinese script form; precipitated on this particle are two smaller particles of θ phase (in white). Fig. 8b corresponds to the same alloy after 5 h of solution treatment at 500°C. In this micrograph, the β phase has been partially substituted by small Q phase particles. The equilibrium of the two phases changed with the annealing temperature. At the lowest solution treatment temperature, the stability of the Q phase reached its maximum and that of the β phase its minimum. In contrast, in the two step solution treatment that finishes at 535°C, the Q phase lost stability, almost disappearing, and a slight increment in the amount of the β phase was found, exactly as predicted by Thermo-Calc.

The amount of the π phase was nearly constant at all of the solution temperatures used. There was no appreciable dissolution of this phase even after 24 h in the salt bath. The stability of this phase was also well predicted by Thermo-Calc. The DSC peak corresponding to the melting of this phase coincided with the mayor Al-Si eutectic melting peak and was completely covered by it, making it impossible to evaluate the evolution of this phase with the DSC. The same difficulty was found in the rest of the alloys studied as described in the following section.

3.2.2. Alloys H4, E and Thixo477

The results of the metallographic measurements and DSC peak energies corresponding to alloys H4 (permanent mould cast), E (lost-foam) and Thixo477 (thixoforming) are shown in Figs 9–11 respectively. The main intermetallic phase in these alloys was θ, as reported in Table II. During solution treatment this phase dissolved progressively in the three alloys. The analysis of the curves demonstrates that the effect of the processing route on the dissolution speed of the θ phase was very strong. In Fig. 12 the evolution of the θ phase at 500°C, as measured metallographically, for the three alloys is shown. Alloy H4 reached equilibrium dissolution after around 2–3 h. The increased dendrite arm spacing and

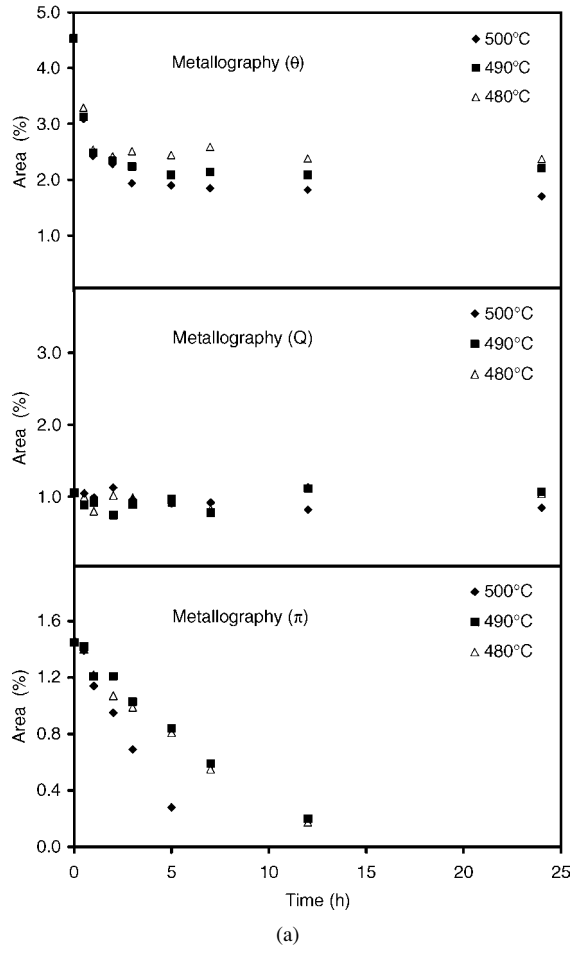

(a)

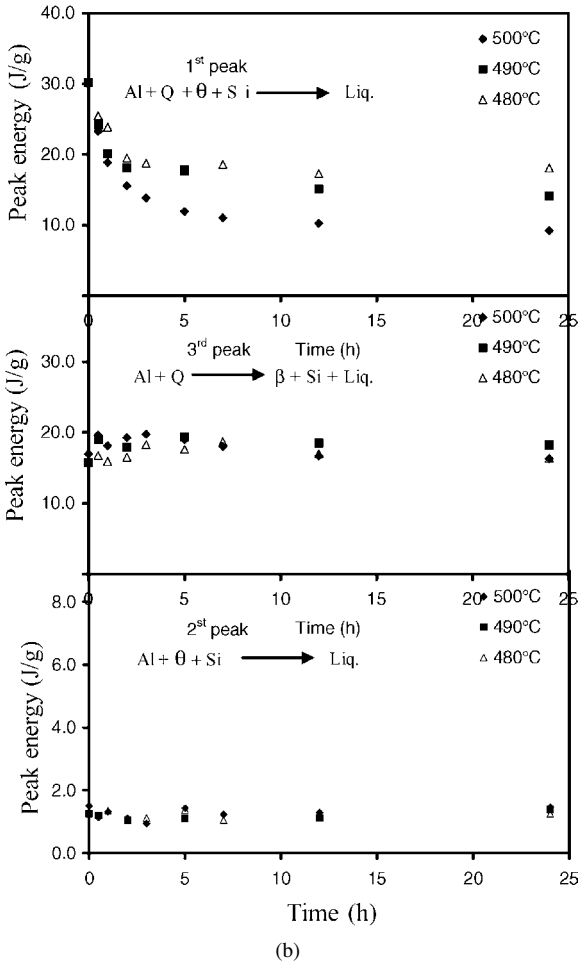

(b)

Figure 9 Evolution of the main intermetallic phases in alloy H4: (a) metallography and (b) DSC.

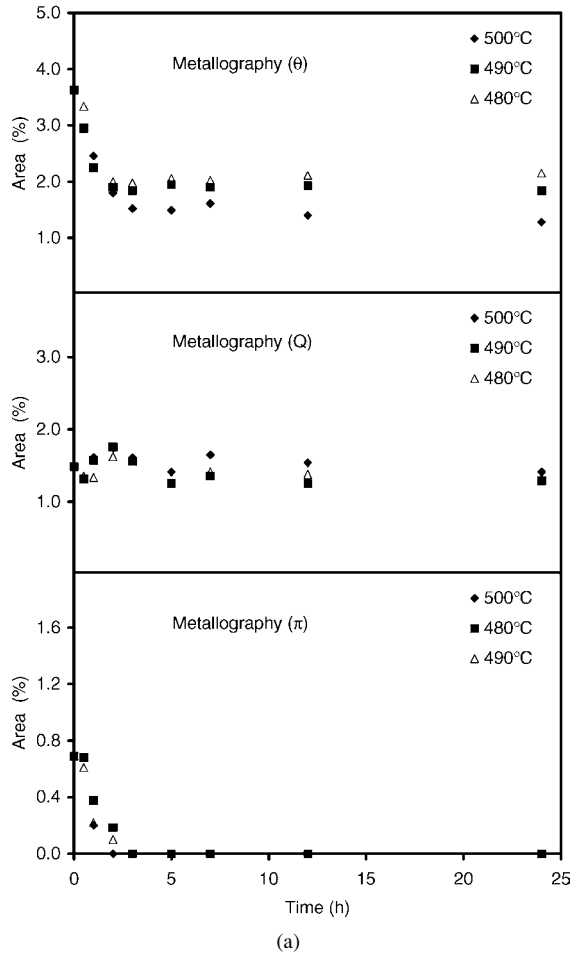

(a)

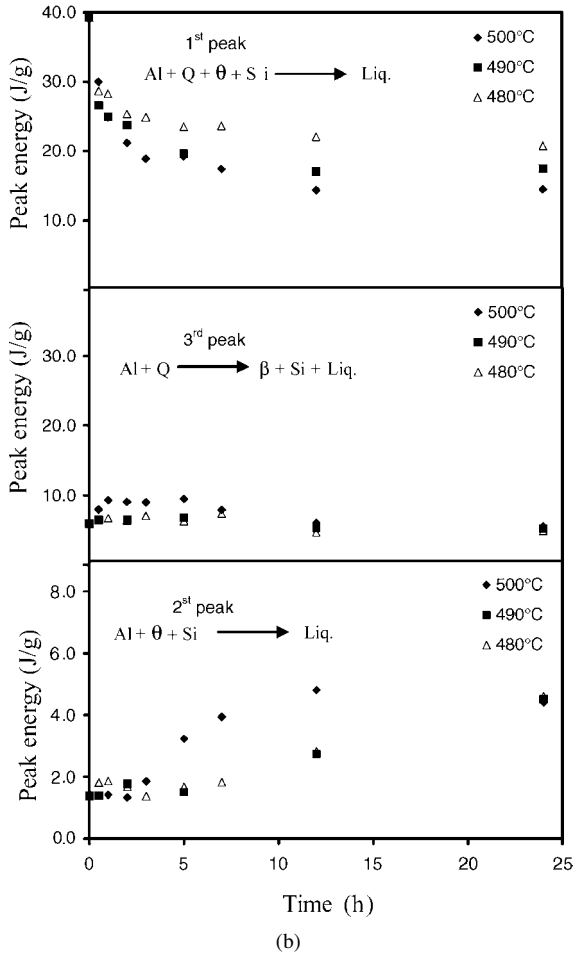

(b)

Figure 10 Evolution of the main intermetallic phases in alloy E: (a) metallography and (b) DSC.

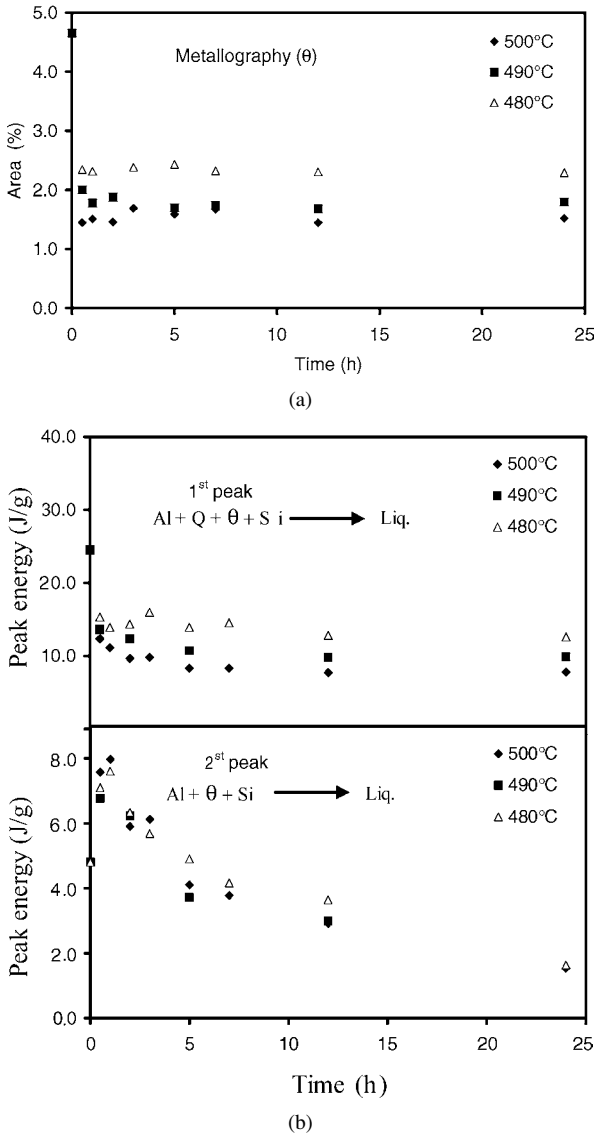

Figure 11 Evolution of the main intermetallic phases in alloy Thixo477: (a) metallography and (b) DSC.

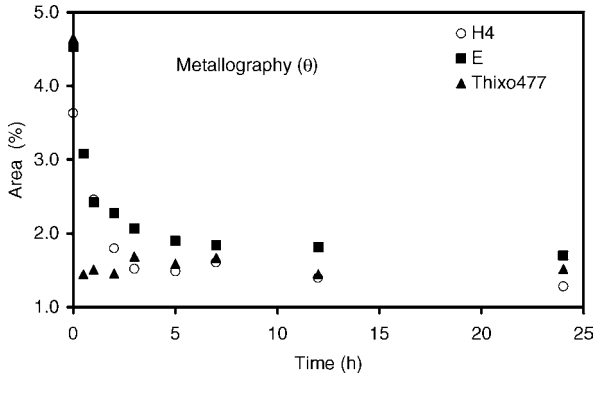

Figure 12 Evolution of the θ phase during solution treatment at 500°C for alloys H4, E and Thixo477.

coarser size of the θ phase in alloy E slowed down the dissolution process slightly. A minimum of 5 h was necessary in this alloy to reach equilibrium. The dissolution of the θ phase in alloy Thixo477 was much faster due to its finer microstructure. The particles dissolved very fast and after only 30–60 min, the dissolution process was in equilibrium. No further dissolution was detected after that time in any of the three solution temperatures studied.

The θ phase in these alloys forms and dissolves following two different reactions from Table III: (θ_a) from reaction (a) and (θ_c) from reaction (c) [21]. Through metallographic examination, in most cases it was possible to differentiate between the two forms because the θ phase from reaction (a) was associated with particles of the Q phase. However, it was not possible to give a quantitative measurement of these two θ phase forms independently using metallography.

The DSC allowed independent monitoring of the evolution of each form. The energy of the first peak in the DSC runs corresponds to the melting of θ_a particles and the second to the melting of the blocky like θ_c particles. The evolution of the second DSC peak during the solution treatment was very different in each alloy. In alloy H4 the energy of the peak remained nearly constant during annealing (Fig. 9). In alloy E there was a marked energy increment of the peak with annealing time; the increment rate was more pronounced at higher treatment temperatures (Fig. 10). Finally in alloy Thixo477 the energy of the peak went up during the first hour, but after this time, it started to decrease smoothly (Fig. 11).

In order to understand the evolution of the second DSC peak and, in consequence, the evolution of the θ_c particles during annealing, the evolution of the π phase must be also analyzed.

Thermo-Calc predicted complete stability of the π phase in the four alloys considered (see Fig. 6). Metallographic examination revealed that in alloy H3 this phase remained stable even after annealing the alloy at 535°C. However in the higher copper content alloys, H4, E and Thixo477, metallographic examination revealed that during solution treatment, the π phase dissolved and simultaneously small Al_2Cu particles formed surrounding the dissolving π particles, as can be seen in the two micrographs of Fig. 13. This process was similar to the dissolution of the β phase previously described for alloy H3. The energy changes of the 2nd DSC peak mentioned earlier, can be explained analyzing the evolution of the π phase during solution treatment.

In alloy H4 the amount of this phase was small compared to that of alloys E and Thixo477. In the latter two, the iron content was higher and the main magnesium containing intermetallic phase was π rather than Q. During solution treatment most of the particles of the π phase, present in alloy H4, quickly dissolved and the formation of the θ_c particles was insignificant. For this reason the energy of the 2nd DSC peak during the solution treatment remained nearly constant.

In alloy E the amount of the π phase in the as-received condition was higher. Due to the slow solidification rate of the alloy, the particles of this phase were also larger. During solution treatment, the π phase slowly dissolved and θ_c particles formed simultaneously. At higher treatment temperatures, the process accelerated as can be seen in the evolution of the 2nd DSC peak at 500°C in Fig. 10. However, after long solution times (24 h) equilibrium was reached and a similar situation was found at the three treatment temperatures considered:

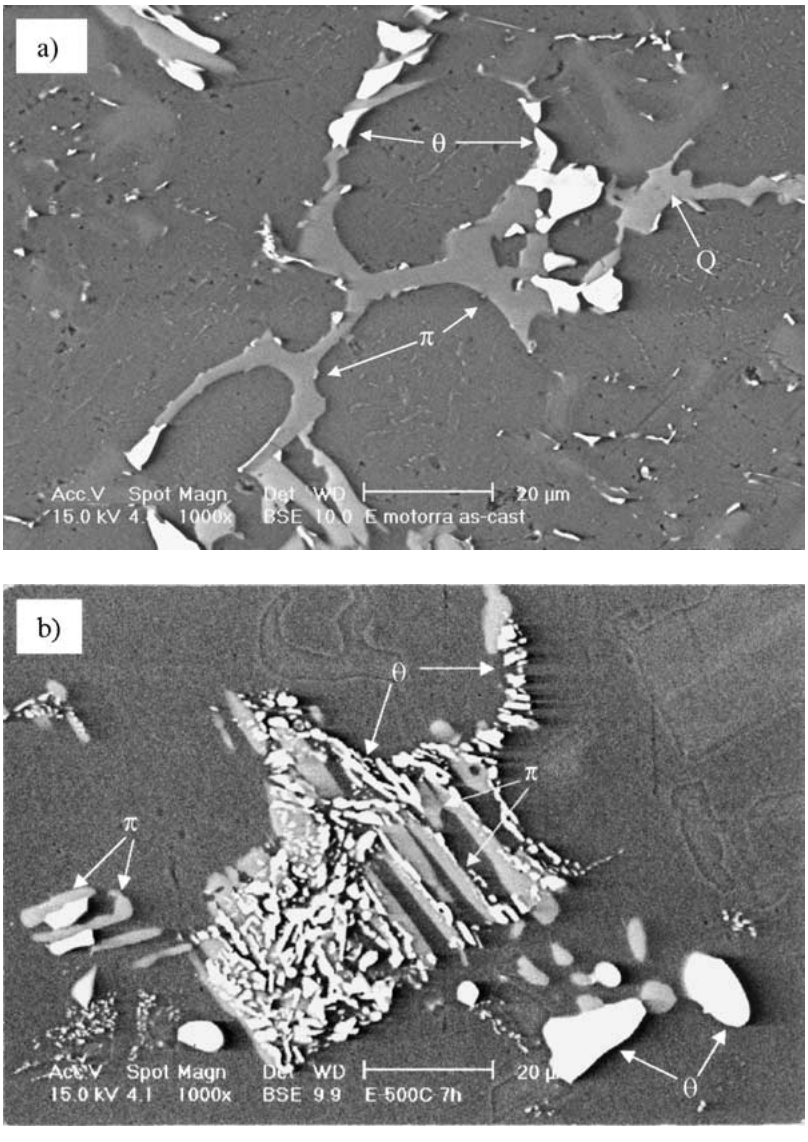

Figure 13 Dissolution of the $Al_8FeMg_3Si_6$ (π) phase and precipitation of the Al_2Cu (θ) phase during solution treatment: (a) alloy E as received and (b) after 7 h at 500°C.

the π phase disappeared almost completely and clusters of small θ particles were formed resembling the shape of the original π particles. Consequently the DSC peak energy at the three solution treatment temperatures was similar after 24 h.

In alloy Thixo477, the π phase was present in the form of very small particles. The small size of these particles promoted very fast dissolution and nucleation of the θ_c particles around them. In Fig. 14, a detail of the formation of θ_c particles in alloy Thixo477 during solution treatment is shown. The process finished after about 1h of solution treatment at all temperatures studied. After this time, progressive dissolution of the small θ_c particles took place. After 24 h of solution treatment these small particles were almost completely dissolved in the matrix. Based on the evolution of the second DSC peak it can be concluded that, the speed of dissolution was similar at the three solution temperatures.

Finally, regarding the evolution of the Q phase in these three alloys, the DSC and metallographic measurements were in total agreement. This phase remained stable during solution treatment in alloys H4 and E. Other researchers have also reported this phase to be insoluble at solution temperatures as high as 530°C in Al-Si-Cu-Mg alloys [25]. However, it must be remembered that the amount of Q phase did change with solution time in the lower copper content alloy H3.

In alloy Thixo477, metallographic examination revealed the presence of a very small fraction of Q particles always associated with θ phase particles. This small fraction reacted completely in the first DSC peak leaving no additional Q phase and consequently inhibiting the apparition of the 3rd DSC peak. This fact was well predicted by Thermo-Calc.

In view of the above observations, it is clear that each of the four alloys requires different solution treatment parameters to optimize the results. As was previously explained, the optimum time at the solution treatment temperature depends upon the alloy composition and fabrication procedure used. The section thickness of the part is also important in determining the time for the solution treatment. The optimum solution times given, are for samples with $15 \times 10 \times 20$ mm approximate dimensions, used in this work. Thicker sections would need longer solution heat treatments [26].

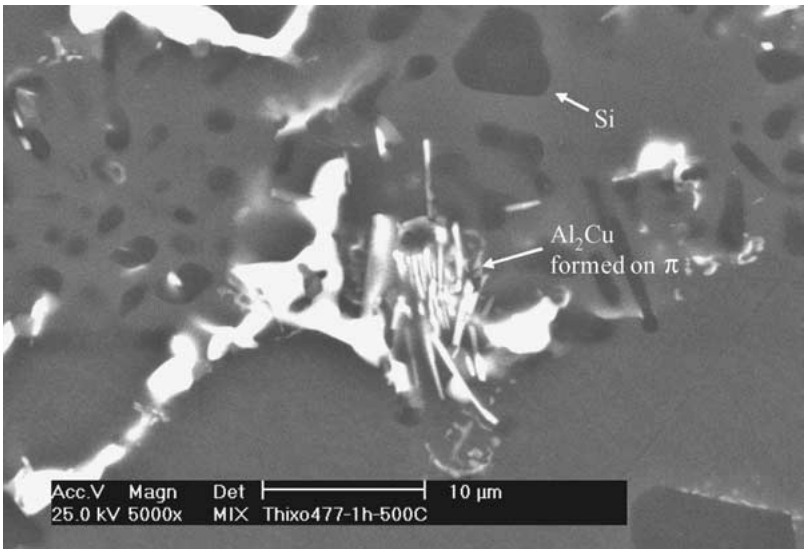

Figure 14 Dissolution of the fine $Al_8FeMg_3Si_6$ (π) phase particles and simultaneous formation of θ phase particles.

In permanent mould cast alloy H3, the optimum solution treatment would be performed in two stages, asfollows: 2.5 h at 500°C followed by 2.5 h at 535°C. At the lower temperature, all the θ phase is placed in solution, permitting a further increase in temperature without any risk of eutectic melting. At 535°C, a more effective dissolution of silicon and magnesium is obtained.

In alloys H4, E and Thixo477, the optimum temperature for the solution treatment is 500°C. The use of slightly higher solution treatment temperatures would only be recommended if the temperature control of the furnace is fine enough to avoid incipient melting (the solidus temperature of these alloys is between 509–510°C). However, the time needed in each alloy varies, due to the different dissolution rate of the θ and π phases.

In permanent mould cast alloy H4, between 2 and 3 h at 500°C are enough to obtain equilibrium dissolution of the θ phase and only 2 h are needed to completely dissolve the π phase. The solution treatment chosen is 2–3 h at 500°C.

Regarding the lost foam alloy E, the coarser size of the intermetallic phases formed during the lost foam process slow down the dissolution kinetics. Consequently, between 5 and 7 h are needed to reach equilibrium dissolution of the θ phase. The π phase dissolves completely after 7 h. The optimum solution treatment for this alloy is 7 h at 500°C.

Finally, in the thixoformed alloy Thixo477, the thin and elongated θ phase particles that coat the aluminum globules in the as-received alloy dissolve extremely fast because the solubility of particles with large surface-to-volume ratios is favored thermodynamically [10]. For the present sample size, only 0.5 to 1 h at 500°C are needed to reach equilibrium.

4. Conclusions

Based on the present findings, the following conclusions can be drawn:

1. The combined use of metallographic measurements and Thermo-Calc calculations allow the identification of the reactions responsible for the endothermic peaks of the DSC runs.
2. Calorimetry was successfully used in monitoring the evolution of the different intermetallic phases during solution treatment. The results obtained agreed well with metallographic measurements and also with calculations of the Thermo-Calc software package.
3. The small compositional changes of alloys H4, E and Thixo477 produce significant variations in the volume fraction of the intermetallic phases. The main intermetallic phase in these alloys is θ.
4. The sluggish solutioning kinetics of alloys E and H4 compared to that of alloy Thixo477 are caused by the extremely fine size of the intermetallic phases found in the thixoformed alloy. Also, the relatively high Mg content of alloy E and especially that of alloy H4 compared to that of alloy Thixo477 causes the formation of a high volume fraction of Q phase particles that remained undissolved during the different solution treatments applied.
5. In alloy H3 the use of a two step solution treatment allows to use a higher solution treatment temperature without any eutectic melting. The use of a higher solution treatment temperature maximizes the dissolution of the magnesium containing intermetallic phases.

Acknowledgments

The alloys were supplied in the framework of an EU-BRITE-EURAM program project (BE96-3652). L. Lasa gratefully acknowledges a research grant from the Basque Government and from the "Fundación de centros Tecnológicos." The authors thank CICYT (project MAT97-1672-CE) for partial funding of the research. The authors would also like to thank Dr. T. Gómez-Acebo for assistance with the Thermo-Calc software, J. M. Martin for fruitful discussions about calorimetry and Dr. N. R. Harlan for a critical reading of the manuscript.

References

1. F. A. DAVIS and T. S. EYRE, *Trib. Int.* **27** (1994) 171.
2. L. LASA and J. M. RODRIGUEZ-IBABE, *Script. Mat.* **46** (2002) 477.
3. B. K. PRASAD, *Mat. Trans. JIM* **35** (1994) 873.
4. F. H. SAMUEL and A. M. SAMUEL, *Metall. Trans.* A **25** (1994) 2247.
5. J. R. DAVIES "Aluminum and Aluminium Alloys" (ASM Specialty Handbook, Ohio. 1993) p. 106.
6. B. K. PRASAD and T. K. DAN, *J. Mater. Sci. Lett.* **10** (1991) 1412.
7. E. CERRI, E. EVANGELISTA, S. SPIGARELLI, P. CAVALIERE and F. DERICCARDIS, *Mater. Sci. Eng.* A **284** (2000) 254.
8. L. LASA and J. M. RODRIGUEZ-IBABE, *Mater. Charac.* **48** (2002) 371.
9. M. GUPTA and E. J. LAVERNIA, *J. Mater. Process. Tech.* **54** (1995) 261.
10. J. CAMPBELL, *Mater. Design* **21** (2000) 373.
11. S. SHIVKUMAR, X. YAO and M. MAKHLOUF, *Script. Mater.* **33** (1995) 39.
12. P. KAPRANOS, D. H. KIRKWOOD, H. V. ATKINSON J. T. RHEINLANDER, J. J. BENTZEN, P. T. TOFT, C. P. DEBEL, G. LASLAZ, L. MAENNER, S. BLAIS, J. M. RODRIGUEZ-IBABE, L. LASA, P. GIORDANO and G. CHIARMETTA, *Int. Conf. Semi-Solid Processing of Alloys and Composites Torino* (2000) p. 741.
13. P. KAPRANOS, D. H. KIRKWOOD, H. V. ATKINSON, J. T. RHEINLANDER, J. J. BENTZEN, P. T. TOFT, C. P. DEBEL, G. LASLAZ , L. MAENNER, S. BLAIS, J. M. RODRIGUEZ-IBABE, L. LASA, P. GIORDANO, G. CHIARMETTA and A. GIESE, Int. Conf. Research and Development in Net Shape Manufacturing, Birmingham (2001).
14. H. KAUFMANN and P. J. UGGOWILTZER, *Advance Eng. Mater.* **3** (2001) 963.
15. K. XIA and G. TAUSIG, *Mater. Sci. Eng.* A **246** (1998) 1.
16. H. KAUFMANN, H. WABUSSEG and P.-J. UGGOWITZER, *Aluminium* **76** (2000) 70.
17. B. SUNDMAN, B. JANSSON and J. O. ANDERSSON, *CALPHAD* **9** (1985) 153.
18. N. SAUNDERS, "TTAl, TT Al-based Alloys Database," (ThermoTech Ltd., Surrey Technology Center, Guildford, UK, 2002).
19. L. F. MONDOLFO, "Aluminum Alloys: Structure and Properties" (Butterworths, London, 1976) p. 644.
20. *Idem*., "Aluminum Alloys: Structure and Properties" (Butterworths, London, 1976) p. 645.
21. A. M. SAMUEL, J. GAUTHIER and F. H. SAMUEL, *Metall. Trans.* A **27** (1996) 1785.
22. D. J. CHAKRABARTI and J. L. MURRAY, "Aluminium Alloys: Their Phisical and Mechanical Properties, Part I" (Transtech Publications, Switzerland/Germany/UK/USA, 1996) p. 177.
23. F. H. SAMUEL, A. M. SAMUEL and H. LIU, *J. Mater. Sci.* **30** (1995) 2531.
24. P. OUELLET and F. H. SAMUEL, *ibid.* **34** (1999) 4671.
25. A. K. GUPTA, A. K. JENA and M. C. CHATURVEDI, *Mater. Sci. Tech.* **3** (1987) 1012.
26. H. Y. HUNSICKER "Aluminum, Properties, Physical Metallurgy and Phase Diagrams" Vol. I (ASM, Ohio, 1967) p. 132.

Received 4 December 2002
and accepted 9 October 2003